Construction and Building Materials 359 (2022) 129518

Contents lists available at ScienceDirect

Construction and Building Materials

journal homepage: www.elsevier.com/locate/conbuildmat

Determination of compressive strength of perlite-containing slag-based geopolymers and its prediction using artificial neural network and regression-based methods

Erdinc H. Alakara [a,b], Sinan Nacar [a], Ozer Sevim [c,*], Serdar Korkmaz [b,d], Ilhami Demir [c]

[a] Department of Civil Engineering, Tokat Gaziosmanpasa University, Tokat 60150, Türkiye
[b] Institute of Science, Kırıkkale University, Kırıkkale 71451, Türkiye
[c] Department of Civil Engineering, Kırıkkale University, Kırıkkale 71451, Türkiye
[d] Department of Construction Technology, Kırsehir Ahi Evran University, Kırsehir 40360, Türkiye

ARTICLE INFO

Keywords:
Geopolymer
Compressive strength
Perlite powder
Artificial neural network (ANN)
Multivariate adaptive regression splines (MARS)
Conventional regression analysis (CRA)

ABSTRACT

This study has two main objectives: (i) to investigate the parameters affecting the compressive strength (CS) of perlite-containing slag-based geopolymers and (ii) to predict the CS values obtained from experimental studies. In this regard, 540 cubic geopolymer samples incorporating different raw perlite powder (RPP) replacement ratios, different sodium hydroxide (NaOH) molarity, different curing time, and different curing temperatures for a total of 180 mixture groups were produced and their CS results were experimentally determined. Then conventional regression analysis (CRA), multivariate adaptive regression splines (MARS), and TreeNet methods, as well as artificial neural network (ANN) methods, were used to predict the CS results of geopolymers using this experimentally obtained data set. Root mean square error (RMSE), mean absolute error (MAE), scatter index (SI) and Nash-Sutcliffe (NS) performance statistics were used to evaluate the CS prediction capabilities of the methods. As a result, it was determined that the optimum molarity, curing time, and curing temperature were 14 M, 24 h, and 110 ℃, respectively and 48 h of heat curing did not have a significant effect on increasing the CS of the geopolymers. The highest performances in regression-based models were obtained from the MARS method. However, the ANN method showed higher prediction performance than the regression-based methods. Considering the RMSE values, it was seen that the ANN method made improvements by 24.7, 2.1, and 13.7 %, respectively, compared to the MARS method for training, validation, and test sets.

1. Introduction

Concrete produced with ordinary Portland cement (OPC) is the most used construction building material in the construction industry. However, OPC is responsible for 6–9 % of greenhouse gases [1,2]. Carbon emissions have raised awareness among researchers, therefore researchers investigated different materials that can be used instead of OPC. Today, geopolymers are seen as an alternative to OPC-based composites. Geopolymers are of great interest to researchers due to their superior mechanical, and durability properties [3,4], as well as global greenhouse gas emission reduction. The name geopolymer was first introduced by Davidovits [5,6]. Geopolymer materials belong to the family of alkali-activated materials and might be fabricated by polymerizing various types of aluminosilicates with activation methods utilizing soluble silica, and the greatly alkali activator solution [7–12]. Natural materials such as clay and kaolin, industrial by-products, which are fly ash, blast furnace slag, and silica fume, are used as aluminosilicate precursors. Sodium hydroxide (NaOH), sodium silicate (Na_2SiO_3), potassium hydroxide (KOH), potassium silicate (K_2O_3Si), and their combinations are commonly used for alkali activator solutions [13]. Geopolymers are achieved through the activation of a precursor with an alkaline solution under an appropriate temperature environment [8,14,15], which is known as geopolymerization. The polysialate 3D networks of monomers occur through geopolymerization consisting of SiO_4 and AlO_4 tetrahedrons [7,14]. The inorganic compounds are composed after complicated chemical reactions between the aluminosilicate precursor oxides in greatly alkaline to generate 3D polymeric Si–O–Al–O chains as the primary alkaline-aluminosilicate gel during the

* Corresponding author.
E-mail address: ozersevim@kku.edu.tr (O. Sevim).

https://doi.org/10.1016/j.conbuildmat.2022.129518
Received 21 July 2022; Received in revised form 20 September 2022; Accepted 16 October 2022
Available online 26 October 2022

Table 1
The chemical composition and physical properties of GBFS and RPP.

Chemical composition (%)	GBFS	RPP
SiO_2	36.12	73.88
Al_2O_3	15.20	15.81
Fe_2O_3	0.62	0.32
CaO	36.10	0.83
MgO	5.64	–
K_2O	0.83	5.21
Na_2O	0.31	3.51
SO_3	1.21	0.08
Physical properties		
Density (g/cm^3)	2.88	2.37
Specific surface area (cm^2/g)	5220	3460
LOI (%)	1.09	–

geopolymerization [7,14,16,17]. The amorphous aluminosilicate gels (N,K-A—S—H) are constructed as a consequence of the chemical reaction (geopolymerization) of aluminosilicates with low CaO/SiO_2 ratios, such as clay and class F fly ash while calcium aluminosilicate hydrate (C-A—S—H) gels are constructed as a consequence of the geopolymerization of aluminosilicates with high CaO/SiO_2 ratios, such as slag and class C fly ash [7,18,19,20,21]. At low alkaline content, sodium is partially replaced by calcium, forming C-(N)-A—S—H gels [7]. Strength development in geopolymer composites depends on N-A—S—H or/and C-A—S—H rather than C—S—H as in traditional cementitious composites [7,14].

Geopolymers have positive properties such as good abrasion resistance, fire resistance, high resistance to acid and salt solutions, low thermal conductivity, low shrinkage as well as high early compressive strength (CS), which is usually the most significant parameter in the construction industry [4,10,11,12,16,17]. There are many factors that affect the CS of geopolymers. The literature studies showed that precursor type and amount, alkali activator type and molarity amount, curing temperature, curing time, and curing environment affected the CS of geopolymer mortars [22–27].

The modeling studies in the literature have been conducted using existing experimental data in order to make this process easier, which is difficult in terms of time, material, equipment, cost, and labor. In the studies, mechanical properties of concrete and geopolymers such as CS, flexural and tensile strength were discussed [28–33]. Artificial intelligence techniques are used to predict engineering properties around the world [34]. Various artificial intelligence techniques such as fuzzy interface system (FIS), response surface methodology (RSM), adaptive neuro-fuzzy interface system (ANFIS), artificial neural network (ANN), support vector machine (SVM), particle swarm optimization algorithm (PSOA), back propagation neural network (BPNN), genetic algorithm (GA), genetic programming (GP), and gene expression programming (GEP) are used by researchers. In the literature, it has been stated that applications such as fuzzy logic (FL), artificial intelligence techniques including metaheuristic algorithms, and GEP show good features in overcoming complex engineering problems [35–41]. Another method that is used in modeling studies and gives effective results in solving many engineering problems is the multivariate adaptive regression splines (MARS) method [39–42]. The MARS method is a flexible and fast method for making predictions. It is also seen as an innovative and promising modeling tool [43]. MARS also has advantages such as high dimensional processing capacity, capturing complex relationships, and estimating the contributions of input variables [44,45]. ANNs are another group of these techniques and have been successfully applied in many prediction studies [35]. In general, there are two other commonly used approaches besides ANNs for estimating CS. These are computational modeling and parametric multivariate regression model [46–48]. Such data-driven methods, especially ANN and FL, have become popular.

Estimation of CS of geopolymer concretes is a current research topic and different estimation models such as ANN, ANFIS, Multiple Linear Regression (MLR), and GEP have been used in the studies. In these models, parameters such as coarse aggregate, fine aggregate, curing temperature, curing time, slag amount, and alkali activator amount were used as input parameters [36,37,49–52]. Rahmati and Toufigh [53] estimated the CS of geopolymer concretes exposed to high temperatures using ANN and support vector regression (SVR) models. In the study, parameters such as coarse aggregate, fine aggregate, slag ratio, molarity, sodium silicate, NaOH, curing temperature, and high temperature were used. Although the results obtained from both models are close to each other, it has been reported that the SVR performs better. Ganesh and Muthukannan [54] estimated the CS of fiber-reinforced geopolymer concrete using ANN. In the model, the age of the concrete, curing condition and dosage of fiber are used as input parameters. It has been found that CS can be estimated with high accuracy using the ANN model. Manikandan and Vasugi [55] estimated the slump, CS, split tensile strength, and flexural strength parameters of waste glass powder substituted geopolymer concretes with the ANN model. Waste glass powder replacement ratio and molarity values were used as input parameters in the model. When the results obtained from the estimation and experimental results were compared, it was seen that the results were close to each other. Ahmad et al. [56] used MARS and ANFIS models to estimate the CS of geopolymer concrete. When comparing both models in terms of R^2, RMSE, and MAE, it was concluded that the ANFIS model showed better correlation and less error compared to the MARS model. Britto and Muthuraj [57] used ANN and MARS models to estimate the CS of geopolymer concrete containing bacteria. A total of 84 data were used in the developed model to estimate the CS of the samples cured for 1, 3, 7, 28, 56, and 90 days. 70 % of this data was used for training and 30 % for testing. According to the results obtained from the study, it was determined that the estimation and experimental data were in harmony, and the developed models were robust and reliable. Pham et al. [58] used the ANN model to predict the 28-day CS results of geopolymer concrete from the input components. Data from 190 test samples taken from previous studies in the literature were used to train the ANN model. According to the results, the "trainlm" learning algorithm provided the best prediction results. Having carried out a thorough literature review, there is limited understanding on the prediction of CS by using parameters such as precursor ratio, alkali activator solution molarity, heat curing temperature, and heat curing time, which affect the CS of geopolymers. Moreover, there has been no detailed study on the prediction of CS of perlite-containing geopolymers. In this context, five different RPP replacement ratios (10, 20, 30, 40, and 50 %), three different alkali activator solution molarities (12, 14, and 16 M), two different heat curing times (24, and 48 h), and five different heat curing temperature (60, 80, 90, 100, and 110 ℃) were determined, and the reference and RPP-incorporating slag-based-geopolymers were produced. A total of 540 (180×3) geopolymer mortar samples were prepared, with each mixture group containing 3 cubic samples with dimensions of 50×50×50 mm. Then, the variables used in the preparation of the geopolymers were used as the inputs of the models, the experimentally obtained CS results were used as the model outputs, and prediction models were developed with regression-based CRA, MARS, and TreeNet methods as well as ANN methods. Root mean square error (RMSE), mean absolute error (MAE), scatter index (SI) and Nash-Sutcliffe (NS) performance statistics were used to evaluate the prediction capabilities of the methods.

2. Experimental study

2.1. Materials

In this study, ground blast furnace slag (GBFS) and raw perlite powder (RPP) were used as aluminosilicate precursors. GBFS was obtained from Ereğli iron and steel plant located in Zonguldak (Türkiye).

Table 2
The mixture proportions of the different geopolymers.

Serial name	Molarity (M)	Precursors (g)		Sand (g)	Water (g)	NaOH (g)
		GBFS	RPP			
R-12 M	12	450	0	1350	200.7	108
P1-12 M		405	45	1350	200.7	108
P2-12 M		360	90	1350	200.7	108
P3-12 M		315	135	1350	200.7	108
P4-12 M		270	180	1350	200.7	108
P5-12 M		225	225	1350	200.7	108
R-14 M	14	450	0	1350	196.7	126
P1-14 M		405	45	1350	196.7	126
P2-14 M		360	90	1350	196.7	126
P3-14 M		315	135	1350	196.7	126
P4-14 M		270	180	1350	196.7	126
P5-14 M		225	225	1350	196.7	126
R-16 M	16	450	0	1350	192.6	144
P1-16 M		405	45	1350	192.6	144
P2-16 M		360	90	1350	192.6	144
P3-16 M		315	135	1350	192.6	144
P4-16 M		270	180	1350	192.6	144
P5-16 M		225	225	1350	192.6	144

The calcium aluminosilicate hydrate (C-A—S—H) gels, which are similar to C—S—H that formed during the hydration of Portland cement, are constructed as a consequence of the geopolymerization of GBFS with high CaO/SiO_2 ratios [7,18,19]. Note that the CaO ratio of GBFS is 36.10 %. However, there is a widespread consensus that a precursor containing more than 20 % CaO is not favorable for geopolymerization owing to its quick setting [7]. Therefore, RPP was used substituting up to 50 % by GBFS. Note that the CaO ratio of RPP is 0.83 %. The perlite in the raw (unprocessed) form used in the study was obtained from the perlite aggregate deposits in Çankırı (Türkiye). A ball mill operating at 60 rpm was used to pulverize the perlite aggregates. Before being used ground RPP, it was sieved through a 90-μm sieve, and the material remaining under the sieve was used. As a result of this process, the fineness of RPP was brought to a similar fineness of the cement. The chemical composition and physical properties of GBFS and RPP are given in Table 1.

NaOH with a molecular weight of 40 g/mol with a purity of approximately 99 % was used to produce an alkaline solution in the study. NaOH has demonstrated a higher capability to dissolve aluminate and silicate [7,59,60]. NaOH furthermore raises the pH of the environment and furnishes reactions for the dissolution of Si and Al in the aluminosilicate precursors to acquire desired binding products [14]. It is also a good option for preparing alkaline solutions with sodium silicate (Na_2SiO_3). It increases the compressive strength (CS) of geopolymers and the geopolymerization process [61]. However, it is not cost-effective, and a significant amount of energy is required during its production [62]. At the same time, the alkaline solution with high silica reduces the pH and diminishes the binding between aluminosilicate precursors and the alkaline solution [14]. Therefore, NaOH was chosen in this study. NaOH was supplied as a paillette and used as an activator in the study. CEN reference sand specified in EN 196–1 [63] standard was used in the experiments. Tap water was used as mixing water.

2.2. The preparation of the geopolymer composites

A total of six series of mixtures were prepared for each molar ratio, including one reference (R) series, and five series with RPP at different ratios (10, 20, 30, 40, and 50 %). The mixture proportions of the different geopolymer composite mortars are given in Table 2.

The mixture proportions of geopolymer mortars were chosen the same as EN 196–1 [63] cement mortar mixture and Duxson and Provis [64] technique was used. Duxson and Provis [64] proposed an OPC-based-composites-like mixing technique for geopolymers. In this technique, the dry mixture is combined with an alkaline activator solution to produce geopolymers. From Table 2, it is seen that the water used in the mixture is in different amounts. This is due to the water content in NaOH. As the molarity in the geopolymer mixtures increased, the water content due to the amount of NaOH increased, so the amount of water used in the mixtures was reduced at the same rate. Note that water demonstrates no role in geopolymerization, and it merely enhances the workability of the mixtures. P1, P2, P3, P4, and P5 in Table 2 show that 10, 20, 30, 40, and 50 % RPP replacement for GBFS, respectively. Geopolymer composites, with dimensions of 50×50×50 mm, were produced in an oven (with heat curing) to perform CS in accordance with ASTM C-109 [65]. This study focuses on CS of geopolymer. The CS of geopolymer gives high CS under high-temperature curing between 60 and 110 ℃ and 24- and 48-hours curing time [7,66–69]. Therefore, prepared geopolymer composite mortars were subjected to curing times of 24 and 48 h and curing temperatures of 60, 80, 90, 100, and 110 ℃. Geopolymer properties can be adversely affected at temperatures higher than 110 ℃ and longer curing times. This can cause evaporation of water, change of gel formations, and thus cracks and shrinkage [70–72] Another factor in terms of CS is the alkaline solution molarity. The CS properties of geopolymers enhance with increasing molar ratios; However, the high molar ratio of alkaline solution can cause the dissolving of aluminosilicate precursors and finally decrease the CS of the geopolymers [7,8,73,74]. Accordingly, the molar ratios of alkaline activators in the mixtures were determined as 12, 14, and 16 M. 180 different groups of geopolymer composites were produced with the variables abovementioned, and the production parameters are illustrated in Fig. 1.

As seen in Fig. 1, a total of six different series were prepared with three different molarities, five different curing temperatures, five different RPP replacement ratios, and two different curing times. Using these parameters, the name of each geopolymer composite sample is coded. For example, if the code P2-12 M−24H−60 T is examined, it is understood that the 20 % RPP-based geopolymer composite sample with 12 molarity is heat cured at 60 ℃ for 24 h. In this way, 180 different group codes were produced. Three samples were used for each code, and

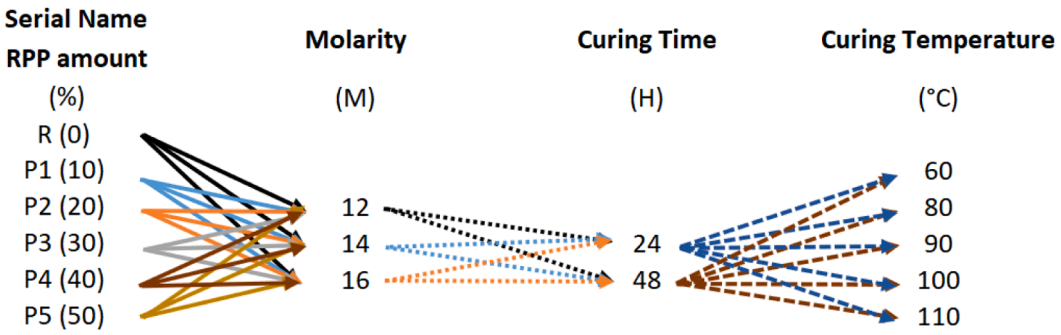

Fig. 1. Production variables of geopolymer composites.

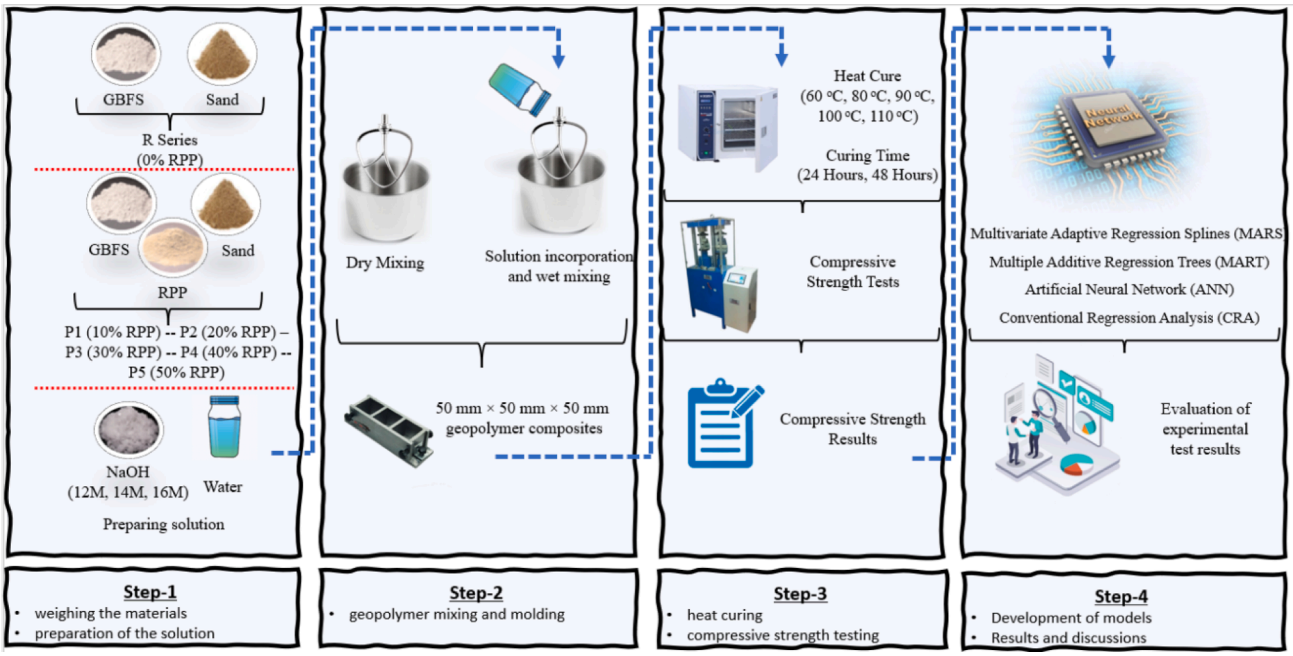

Fig. 2. The production, experimental test, and modeling stages of geopolymer composite mortars.

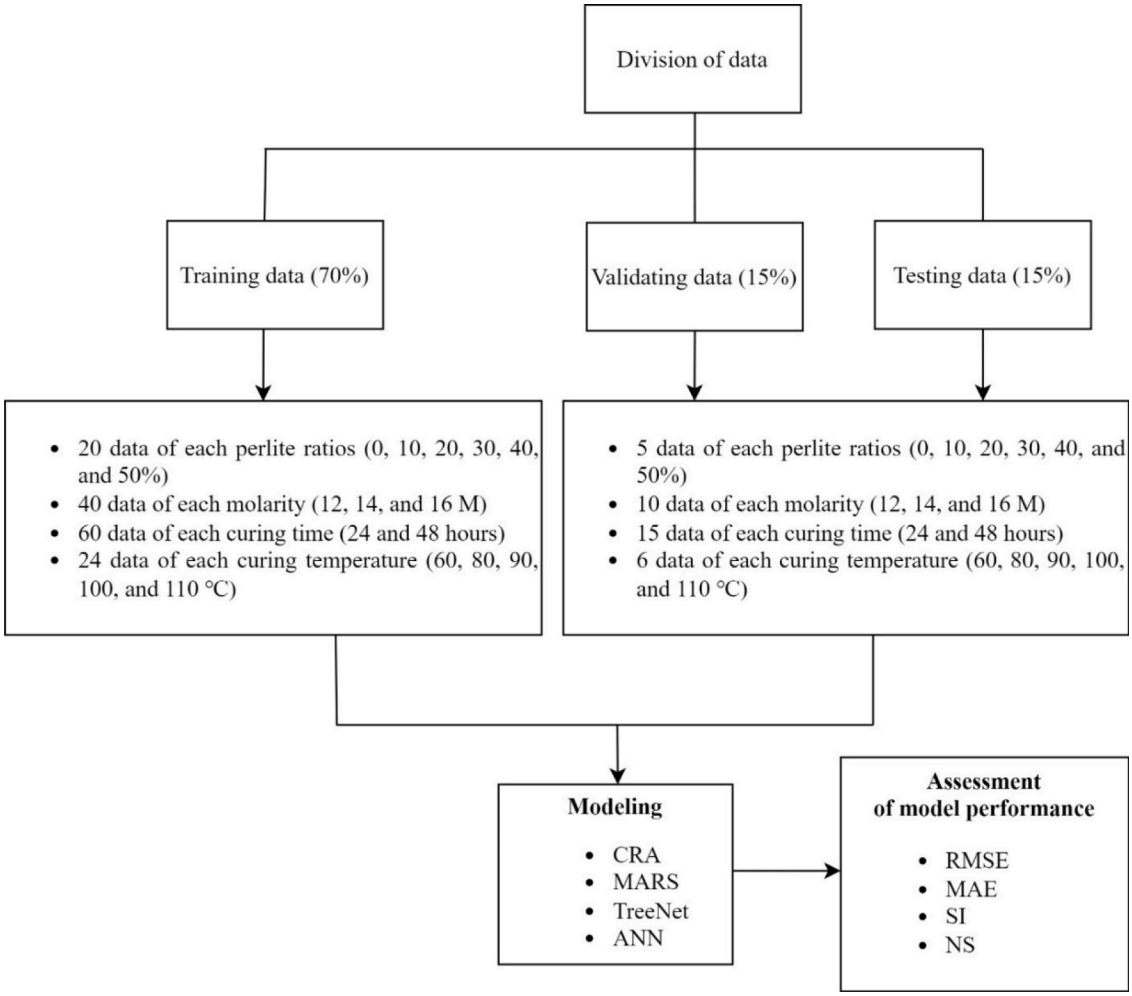

Fig. 3. The flow chart for division of data.

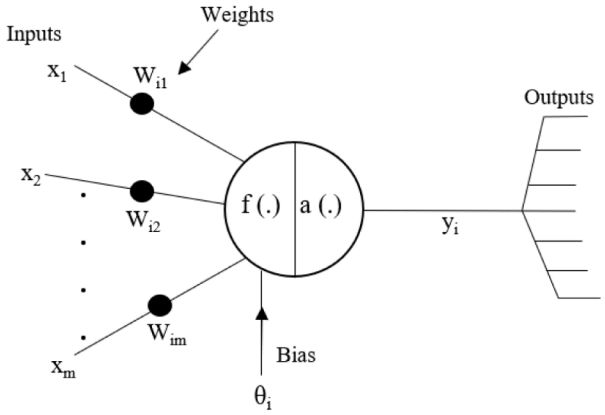

Fig. 4. Artificial neuron model [83].

the average CS result of the three samples was accepted as the final CS result. The CS tests were performed in accordance with ASTM C-109 [65]. Fig. 2 shows the production, experimental test, and modeling stages of geopolymer composite mortars.

3. Methodology of modeling

3.1. Development of models

In the study, a total of 180 different mixtures and 540 geopolymer samples were prepared by using different raw perlite powder (RPP) replacement ratios (0, 10, 20, 30, 40, and 50 %), different molarity ratios (12, 14, 16 M), different curing times (24 and 48 h), and different curing temperatures (60, 80, 90, 100, and 110 ℃). The experimental compressive strength (CS) test results of the 180 mixtures (540 samples) were used in the development of the prediction models. 120 of the obtained results (approximately 70 %) were reserved for training the models, 30 (approximately 15 %) for the validation of the models, and the remaining 30 (approximately 15 %) for the testing of the models. While creating the validation and test data sets, care was taken to represent the entire data group. For this purpose, 5 (6×5) mixtures represent each RPP replacement ratio, 10 (3×10) mixtures represent each molarity, 15 (2×15) mixtures represent each curing time, and 6 (5×6) mixtures represent each curing temperature, a total of 30 mixture validation and test data sets were used. Fig. 3 illustrates the flow chart for data division. In order to facilitate optimization in the modeling stages and to achieve more accurate results, all the data sets were normalized between 0.1 and 0.9 using the equation given in Eq. (1) [42,75].

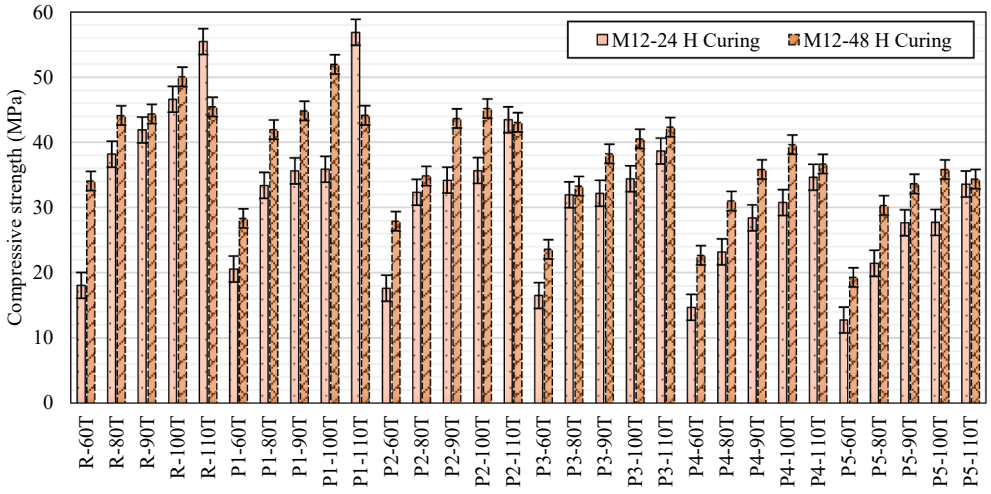

Fig. 5. Compressive strengths of geopolymer composites having 12 molarity.

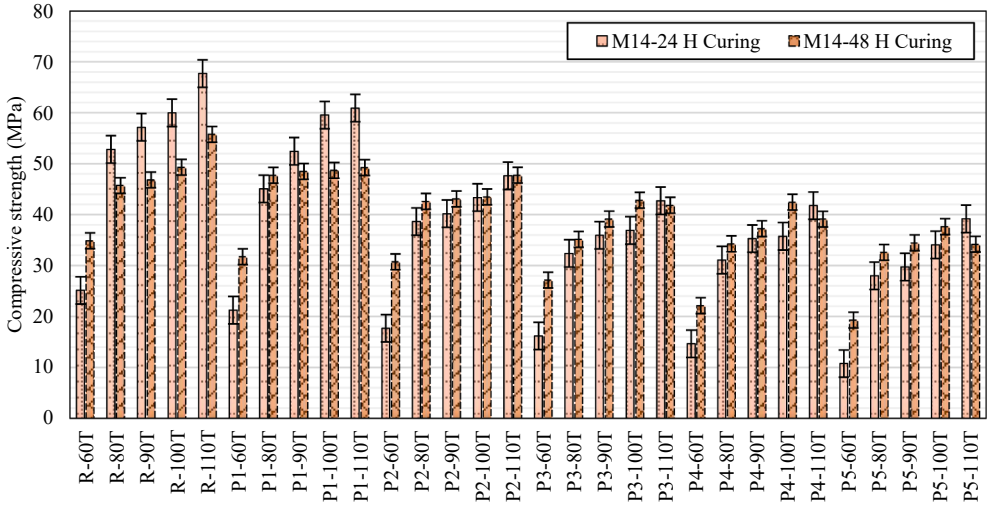

Fig. 6. Compressive strengths of geopolymer composites having 14 molarity.

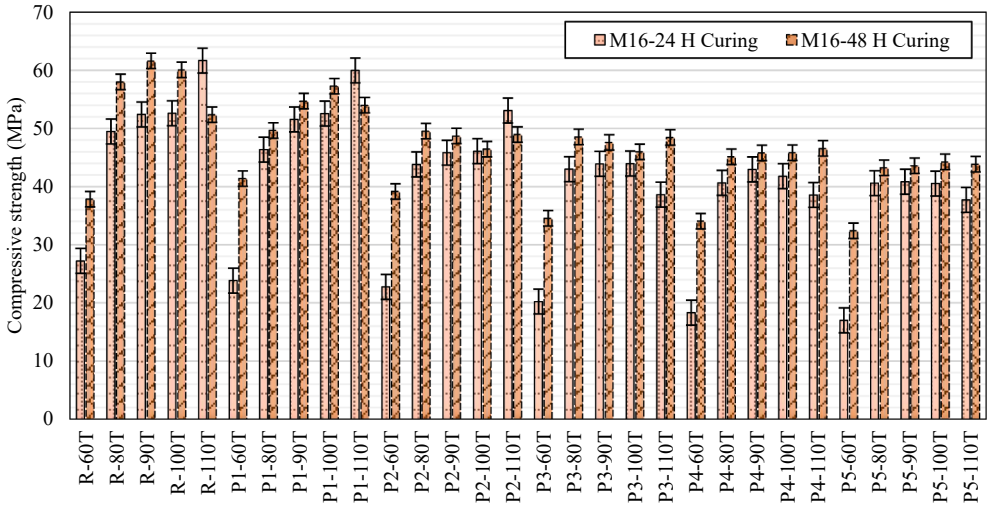

Fig. 7. Compressive strengths of geopolymer composites having 16 molarity.

$$\text{Normalised value} = \left[\frac{\text{Raw value} - \text{Minimum value}}{\text{Maximum value} - \text{Minimum value}}\right] \times (0.8) + 0.1 \tag{1}$$

Then equations and basic functions with the lowest error were determined by applying the regression-based CRA, MARS and TreeNet methods, respectively. MARS, and TreeNet models were implemented using Salford Predictive Modeler 8.0 software. Finally, the ANN method was applied to the same data sets.

3.2. Conventional regression analysis (CRA)

Conventional regression analysis (CRA) is one of the statistical concepts of fitting methods to data from practical problems, validation of the predicted models, and finally extracting useful information from them [76]. In this study, four different regression functions are considered for the CRA method. These functions are linear function (LF), power function (PF), exponential function (EF), and quadratic function (QF). CRA was used to optimize unknown coefficients of independent variables [41]. The LF, PF, EF, and QF can be formulated as follows:

$$y_{LF} = w_0 + w_1x_1 + w_2x_2 + w_3x_3 + w_4x_4 \tag{2}$$

$$y_{PF} = w_0x_1^{w1}x_2^{w2}x_3^{w3}x_4^{w4} \tag{3}$$

$$y_{EF} = w_0 + exp(w_1 + w_2x_1 + w_3x_2 + w_4x_3 + w_5x_4) \tag{4}$$

$$\begin{aligned} y_{QF} =& w_0 + w_1x_1 + w_2x_2 + w_3x_3 + w_4x_4 + w_5x_1x_2 + w_6x_1x_3 + w_7x_1x_4 \\ &+ w_8x_2x_3 + w_9x_2x_4 + w_{10}x_3x_4 + w_{11}x_1^2 + w_{12}x_2^2 + w_{13}x_3^2 + w_{14}x_4^2 \end{aligned} \tag{5}$$

In these equations, w_n regression coefficients, x_n independent variables, and y for CS.

3.3. Multivariate adaptive regression splines (MARS)

MARS is a non-parametric statistical method first proposed by Friedman [43]. The MARS method applies a divide-and-conquer strategy to explain the relationship between variables. The method makes no prior assumptions for functional relationships between dependent and independent variables [45]. Non-parametric regression methods are used to represent nonlinear events between variables. The MARS technique produces flexible, sensitive, and fast regression models to predict continuous and binary output variables [77]. The model uses feed-forward algorithms for variable estimation [41]. The main advantage of the model is its ability to explain the complex and non-linear relationship between the dependent and independent variables [78]. The basic principle of the MARS method is that it divides the data into several regions to fit a regression model for each region. The break values between regions are called "nodes". The term "basis function" (BF) is used to represent each different range of independent variables. BFs are functions (Eq. (6)) of the following form.

$$max(0, x-k) or\, max(0, k-x) \tag{6}$$

where $\times$ is the predictor variable, and k is the threshold value [79]. The general formulation (Eqs. (7) and (8)) of MARS, which consists of a linear combination of BFs, is as follows:

$$y = f(x) + \varepsilon \tag{7}$$

$$f(x) = \beta_0 + \beta_m BF_m(x) \tag{8}$$

where y is the dependent variable estimated by the unknown function $f(x)$ and ε is the error. BFm is the m'th principal function and its coefficient of βm. m is the maximum number of basic functions that fit the data [77].

3.4. TreeNet

TreeNet, also known as multiple additive regression trees (MART) or gradient-boosting decision tree (GBDT), is a method developed by Friedman [80]. TreeNet is a general additive boosting regression model (ABRM) with a decision tree as its core learner. The main difference of TreeNet from other ABRMs is that its core learner is a decision tree, and it can capture a non-linear relationship between dependent and independent variables [81]. The TreeNet technique provides exceptional modeling accuracy, high-speed result generation, and a high degree of fault tolerance in incomplete datasets. The TreeNet model generally consists of several hundred to several thousand small trees, each containing about six terminal nodes. Each tree included in the model makes a small contribution to the overall model, and the final model estimate is the sum of the contributions of all these trees. Therefore, the TreeNet model can be thought of as a black box with extraordinarily accurate results. The model resembles a long series expansion, such as a Fourier or Taylor series, which is a summation of factors that gets more and more accurate as the expansion continues. The expansion can be written as:

$$F(X) = F_0 + \beta_1T_1(X) + \beta_2T_2(X) + \ldots + \beta_MT_M(X) \tag{9}$$

Each T_i represents a small tree in Eq. (9). This should be read as a weighted sum of terms from the appropriate terminal node of each small tree [82].

Table 3
Coefficients obtained from CRA for CS.

Function	Coefficients														
	w_0	w_1	w_2	w_3	w_4	w_5	w_6	w_7	w_8	w_9	w_{10}	w_{11}	w_{12}	w_{13}	w_{14}
LF	0.324	−0.296	0.161	0.064	0.390										
PF	0.609	−0.202	0.108	0.036	0.324										
EF	−22.571	3.131	−0.013	0.007	0.003	0.017									
QF	−21.302	−0.288	0.147	238.342	1.112	−0.004	0.079	−0.256	−0.019	−0.001	−0.263	0.106	0.028	−238.158	−0.471

3.5. Artificial neural network (ANN)

The ANN is an information processing method inspired by biological systems such as the brain. Neural networks consist of a large number of processing elements (neurons) that work in harmony to solve specific problems. A schematic diagram for an artificial neuron model is shown in Fig. 4. Neurons are connected to each other through directed connections. Each link has a weight associated with it. ANN has the logic to find the most effective solution based on past experience when unknown data is entered into the network [83,84]. The output of the neuron network is given in Eq. (10).

$$y(t+1) = a\left(\sum_{j=1}^{m} w_{ij}x_j(t) - \theta_i\right) \text{ and } f_i \triangleq net_i = \sum_{j=1}^{m} w_{ij}x_j - \theta_i \tag{10}$$

where $X = (X_1, X_2, \ldots, X_m)$ represents the input m applied to the neuron. W_i represents the weights for the input X_i. θ_i is the effect value. $a(.)$ is the activation function. Some issues should be considered while installing the ANN model. First, the appropriate structure of the model should be selected, and the activation function and activation values should be determined. Layer numbers and the number of units for each layer should be selected. ANN models are used in areas such as model matching, nonlinear system modeling, power generation, communications, the electrical and electronics industry, medical applications, the chemical industry, and data mining due to their parallel processing capabilities [83].

3.6. Assessment of model performance

The prediction performances of the methods were evaluated using RMSE, MAE, SI, and NS statistics given in Eqs. (11) to (14).

$$\text{RMSE} = \sqrt{\frac{1}{N}\sum_{i=1}^{N}(t_i - td_i)^2} \tag{11}$$

$$\text{MAE} = \frac{1}{N}\sum_{i=1}^{N}|(t_i - td_i)| \tag{12}$$

$$\text{SI} = \frac{\text{RMSE}}{\bar{t}} \tag{13}$$

$$\text{NS} = 1 - \frac{\sum_{i=1}^{N}(t_i - td_i)^2}{\sum_{i=1}^{N}(t_i - \bar{t}_-)^2} \tag{14}$$

Here, t_i is the experimental CS values, $\bar{t}$ is the mean of these values, td_i is the value obtained from the model, and N is the number of observations. NS takes a value between $-\infty$ and 1. The fact that NS = 1 indicates that the method is a physical and perfect method. On the other hand, Moriasi et al. [85] have proposed a range for NS statistics that determines the level of proficiency of model performance. Accordingly, if the NS value is 0.75–1, 0.65–0.75, 0.50–0.65, and <0.50, the model performance is classified as very good, good, sufficient, and unsatisfactory, for these ranges, respectively. The closer the NS value is to 1, the higher the model performance.

4. Results and discussion

4.1. Evaluation of experimental results

A total of 180 different mixtures and 540 geopolymer samples were produced according to the stages shown in Fig. 2 and subjected to compressive strength (CS) tests. The CS test results of samples are presented in Figs. 5-7.

As seen in Fig. 5, test results of the geopolymers produced in 12 M show that the highest and lowest CSs are P1-12 M−24H−110 T and P5-

Table 4
Performance of MARS models predicted CS for different values of variables.

Model	M1	M2	M3	M4	M5	M6	Training				Validating				Testing			
							RMSE	MAE	SI	NS	RMSE	MAE	SI	NS	RMSE	MAE	SI	NS
1	4	4	18	7	3	−5	2.648	2.107	0.068	0.947	3.616	2.625	0.094	0.863	3.328	2.694	0.085	0.916
2	4	4	18	2	6	−2	2.842	2.235	0.072	0.940	2.979	2.236	0.077	0.907	3.090	2.475	0.078	0.925
3	4	4	20	3	5	−5	2.269	2.079	0.068	0.946	3.356	2.572	0.087	0.882	3.085	2.747	0.078	0.926
4	4	4	20	5	5	−2	3.016	2.399	0.077	0.933	3.029	2.306	0.078	0.904	3.034	2.424	0.077	0.928
5	4	4	24	5	2	−2	3.169	2.506	0.081	0.926	2.717	2.019	0.070	0.923	3.172	2.238	0.081	0.921
6	4	4	24	8	5	−3	2.748	2.161	0.070	0.944	2.905	2.159	0.075	0.912	3.349	2.546	0.085	0.912
7	4	4	30	6	3	−4	3.163	2.491	0.080	0.926	2.680	2.021	0.069	0.925	3.151	2.262	0.080	0.922
8	4	4	30	2	2	−5	2.462	1.922	0.063	0.955	3.213	2.364	0.083	0.892	3.278	2.689	0.083	0.916
9	4	4	36	2	6	−5	3.287	2.578	0.083	0.920	3.166	2.373	0.082	0.895	3.068	2.392	0.078	0.926
10	4	4	36	8	3	−1	3.564	2.880	0.091	0.906	3.236	2.577	0.084	0.890	3.575	2.621	0.091	0.900
11	4	4	40	6	3	−7	3.163	2.491	0.080	0.926	2.679	2.022	0.069	0.925	3.151	2.263	0.080	0.922
12	4	4	40	2	7	−2	3.094	2.391	0.079	0.929	3.136	2.404	0.081	0.897	3.124	2.382	0.079	0.924
The Best	**4**	**4**	**28**	**6**	**4**	**−4**	**2.348**	**1.758**	**0.060**	**0.959**	**2.498**	**1.742**	**0.065**	**0.935**	**2.895**	**2.204**	**0.074**	**0.934**

Table 5
Basis functions and equations obtained from MARS for CS.

BF1	max (0, T* − 0.42)	BF16	max (0, M − 0.1) × BF1
BF2	max (0, 0.42 − T)	BF17	max (0, T − 0.1) × BF4
BF3	max (0, P* − 0.1)	BF19	max (0, 0.26 − P) × BF16
BF4	max (0, M* − 0.1)	BF20	max (0, H − 0.1) × BF13
BF5	max (0, H* − 0.1) × BF2	BF21	max (0, P − 0.26) × BF17
BF6	max (0, P − 0.1) × BF2	BF23	max (0, H − 0.1)
BF7	max (0, H − 0.1) × BF3	BF24	max (0, H − 0.1)
BF8	max (0, T − 0.42) × BF7	BF25	max (0, 0.5 − M) × BF23
BF13	max (0, 0.42 − P) × BF1	BF26	max (0, T − 0.74) × BF23
BF15	max (0, 0.5 − M) × BF13	BF27	max (0, 0.74 − T) × BF23
		BF28	max (0, M − 0.1) × BF5

$$CS = 0.480907 + 0.368676 \times BF1 - 0.673489 \times BF2 - 0.295835 \cdot BF3 + 0.0657375 \times BF4 + 0.303429 \times BF6 + 0.148339 \times BF8 + 2.18153 \times BF13 - 4.66326 \times BF15 - 0.96805 \times BF16 + 0.527518 \times BF17 - 3.16055 \times BF19 - 0.896384 \times BF20 + 0.199104 \times BF21 + 0.141131 \times BF24 + 0.16082 \times BF25 - 0.393213 \times BF26 + 0.154137 \times BF27 + 0.423124 \times BF28.$$

*T, H, M, and P represent curing temperatures, curing times, molarity, and perlite, respectively.

12 M−24H−60 T geopolymers, respectively. By increasing the curing time of geopolymer composites cured at 60 ℃ from 24 h to 48 h, significant increases were observed in CSs of all RPP-based geopolymer composite series. This situation was consistent with the studies in the literature [86,87]. The CSs of geopolymer composites cured at 110 ℃ curing temperature in the R, P1, and P2 series have higher CS results than the geopolymers produced in the same series, which are cured at 110 ℃ curing temperature for 48 h. This might be attributed to precursor reactivity and the geopolymerization process enhanced at high-temperature curing [7,14]. It has been observed that the curing temperature should be increased in order to increase the CS rapidly. As a result, it was revealed that short curing times at high temperatures had a positive effect on CS. This might be attributed that geopolymer gels begin to deteriorate and cracks occur during long curing times under high temperatures [70–72].

As seen in Fig. 6, test results of the geopolymers produced in 14 M show that the CS of all RPP-based geopolymer series increased by increasing the molarity ratio from 12 to 14. In geopolymer composites with 14 M, the highest CS was obtained with R-14 M−24H−110 T cured at 110 ℃ for 24 h. An increase of 22.08 % was achieved in the CS of the R series produced under the same conditions with the increase in molarity. As a result, with the increase of molarity, significant increases occurred in the CS of the samples, especially those cured for 24 h. The highest CS results were also obtained in the 24-hour curing condition. The CS properties of geopolymers enhance with increasing molar ratios [7,73,74]. This is because the geopolymerization process increases with the increase in molarity. This can be attributed to more Si and Al dissolving from aluminosilicate precursors, and the chemical geopolymerization process is enhanced with high molarity.

As seen in Fig. 7, test results of the geopolymers produced in 16 M show that the geopolymer composites with 16 M reached higher CS results than the geopolymers produced in 14 M at 60 and 80 ℃ heat curing. It was determined that increasing the molarity from 14 to 16 had the most positive effect on the CS at 60 ℃. The CSs of the R, P1, P2, P3, P4, and P5 series cured at 60 ℃ for 48 h increased by 8.53, 30.37, 27.36, 27.31, 53.86, and 67.93 %, respectively. It has been observed that RPP has a positive effect on CS at only low curing temperatures. The same effect was not observed at high curing temperatures. This is because GBFS is more active than RPP at high curing temperatures. This demonstrates that the degree of geopolymerization of GBFS is much higher than that of RPP. As a result, while the increase in molarity in the production of geopolymer composites had a positive effect on the CS of

Table 6
Performance of TreeNet models predicted CS for different values of variables.

Model	T1	T2	T3	T4	T5	Training				Validating				Testing			
						RMSE	MAE	SI	NS	RMSE	MAE	SI	NS	RMSE	MAE	SI	NS
1	0.50	10,000	6	10,000	10	3.594	2.574	0.091	0.904	3.218	2.456	0.083	0.891	3.679	2.763	0.093	0.894
2	0.50	10,000	3	45,000	1	3.625	2.435	0.092	0.903	3.075	2.347	0.080	0.901	3.639	2.789	0.092	0.896
3	0.55	10,000	4	15,000	3	3.204	2.105	0.081	0.924	2.880	2.097	0.075	0.913	3.267	2.519	0.083	0.916
4	0.60	10,000	5	25,000	7	3.284	2.200	0.083	0.920	3.032	2.194	0.079	0.904	3.518	2.629	0.089	0.903
5	0.65	10,000	8	10,000	5	2.781	1.913	0.071	0.943	2.879	2.113	0.075	0.913	3.170	2.440	0.081	0.921
6	0.70	10,000	2	50,000	5	4.797	3.210	0.122	0.830	3.271	2.711	0.085	0.888	4.227	3.302	0.107	0.860
7	0.75	10,000	7	20,000	3	2.903	1.860	0.074	0.938	2.802	2.057	0.073	0.918	3.297	2.577	0.084	0.915
8	0.75	10,000	9	40,000	2	2.743	1.796	0.070	0.944	2.777	2.029	0.072	0.919	3.234	2.534	0.082	0.918
9	0.80	10,000	6	10,000	8	3.207	2.133	0.081	0.924	2.910	2.076	0.075	0.911	3.391	2.706	0.086	0.910
10	0.90	10,000	5	30,000	4	3.123	2.045	0.079	0.928	2.865	2.132	0.074	0.914	3.493	2.785	0.089	0.904
11	1.00	10,000	8	35,000	6	2.973	1.916	0.076	0.935	3.221	2.267	0.083	0.891	3.344	2.596	0.085	0.912
12	1.00	10,000	10	10,000	10	2.908	1.879	0.074	0.937	3.078	2.372	0.080	0.901	3.131	2.393	0.080	0.923
The Best	**0.60**	**10,000**	**10**	**25,000**	**1**	**2.476**	**1.687**	**0.063**	**0.955**	**2.742**	**2.020**	**0.071**	**0.921**	**3.093**	**2.239**	**0.079**	**0.925**

Table 7
Performance values of ANN models for different neuron numbers in the hidden layer.

Number of neurons	Training				Validating				Testing			
	RMSE	MAE	SI	NS	RMSE	MAE	SI	NS	RMSE	MAE	SI	NS
4	2.760	2.045	0.070	0.944	3.508	2.734	0.091	0.871	3.530	2.454	0.090	0.902
5	2.162	1.591	0.055	0.965	2.861	2.163	0.074	0.914	3.048	2.379	0.077	0.927
6	2.202	1.710	0.056	0.964	2.736	2.133	0.071	0.922	3.068	2.465	0.078	0.926
7	2.094	1.624	0.053	0.968	3.066	2.315	0.079	0.901	3.178	2.462	0.081	0.921
8	1.991	1.457	0.051	0.971	2.757	2.049	0.071	0.920	2.679	2.287	0.068	0.944
9	1.933	1.406	0.049	0.972	2.961	2.251	0.077	0.908	3.043	2.445	0.077	0.928
10	1.772	1.300	0.045	0.977	2.946	2.220	0.076	0.909	2.760	2.259	0.070	0.940
12	1.801	1.295	0.046	0.976	2.804	2.292	0.073	0.918	3.128	2.581	0.079	0.923
14	**1.768**	**1.324**	**0.045**	**0.977**	**2.446**	**1.974**	**0.063**	**0.937**	**2.498**	**2.090**	**0.063**	**0.951**
16	1.883	1.405	0.048	0.974	3.152	2.498	0.082	0.896	2.845	2.450	0.072	0.937
18	1.889	1.354	0.048	0.974	3.037	2.416	0.079	0.903	2.924	2.450	0.074	0.933
20	2.251	1.718	0.057	0.962	2.705	2.291	0.070	0.923	2.652	1.961	0.067	0.945
25	2.058	1.576	0.052	0.969	2.953	2.367	0.076	0.908	2.779	2.228	0.071	0.939
30	1.960	1.477	0.050	0.972	2.895	2.162	0.075	0.912	2.606	1.981	0.066	0.947
40	2.133	1.554	0.054	0.966	2.961	2.227	0.077	0.908	3.228	2.586	0.082	0.918

Table 8
RMSE, MAE, SI and NS values of ANN, MARS, TreeNet and CRA in training, validating and testing sets.

Data	Performance Statistics/Methods	ANN	MARS	TreeNet	CRA_QF	CRA_PF	CRA_LF	CRA_EF
Training	RMSE	**1.768**	2.348	2.476	3.368	4.681	4.912	4.915
	MAE	**1.324**	1.758	1.687	2.631	3.914	3.871	3.873
	SI	**0.045**	0.060	0.063	0.086	0.119	0.125	0.125
	NS	**0.977**	0.959	0.955	0.916	0.838	0.821	0.821
Validating	RMSE	**2.446**	2.498	2.742	3.813	5.016	5.041	5.809
	MAE	1.974	**1.742**	2.020	2.965	3.967	3.983	4.196
	SI	**0.063**	0.065	0.071	0.099	0.130	0.131	0.150
	NS	**0.937**	0.935	0.921	0.848	0.736	0.734	0.646
Testing	RMSE	**2.498**	2.895	3.093	3.328	4.747	4.762	4.975
	MAE	**2.090**	2.204	2.239	2.540	3.419	3.427	3.792
	SI	**0.063**	0.074	0.079	0.085	0.121	0.121	0.126
	NS	**0.951**	0.934	0.925	0.913	0.824	0.823	0.806

geopolymer composites cured only at low temperatures, it did not have the same positive effect on the CS of geopolymer composites cured at high temperatures. The reason for this situation is the destruction of the geopolymer structure with long-term high-temperature curing [88]. Thus, cracks occur and the strength of the geopolymer composite decreases [70–72,89]. Moreover, this can be attributed that the high molar ratio of alkaline solution can cause the dissolving of aluminosilicate precursors and finally decrease the CS of the geopolymers [7,8,73,74]. It has been observed that geopolymers can achieve high CS in a short time by curing at high temperatures. The CS of geopolymers produced by substituting RPP instead of GBFS (except the P1 series) were lower than the R series in all conditions. This is because the degree of geopolymerization of GBFS is much higher than that of RPP. Additionally, it was demonstrated that NaOH contributed significantly to compressive strength development.

4.2. Evaluation of modeling results

4.2.1. Conventional regression analysis (CRA) modeling results

The CRA method, which includes LF, PF, EF, and QF functions, was used to check the accuracy of the heuristic regression methods and ANN method. The coefficients obtained with the CRA functions are given in Table 3. These coefficients were then used to generate validation and test datasets and the predictive capabilities of the models were compared. Model performance statistics for the CRA method are given in Section 4.2.5.

4.2.2. Multiple adaptive regression splines (MARS) modeling results

The parameters speed factor (M1), degrees of freedom for knot optimization (M2), maximum basis functions (M3), maximum interactions (M4), minimum observations between knots (M5) and ridge (M6) parameters must be selected accordingly in the analyzes made with the MARS method. These parameters affect the performance of the MARS method. In this study, M1 and M2 parameters were selected as 4, while M3, M4, M5, and M6 parameters were selected in the range of 5–50, 1–10, 0–10, and 0– (–9), respectively. The performance of the MARS method for different trials of the parameters is given in Table 4. The basis functions of the model with the best performance and the equation obtained from these functions are given in Table 5. The number of basis functions used to estimate the CS was determined as 28. The basis functions given in Table 5 for the training dataset and the equation obtained from these functions were then used to generate validation and test datasets, and the predictive ability of the model was compared with other models.

4.2.3. TreeNet modeling results

The parameters such as subsample fraction (T1), the number of trees to build (T2), the number of maximum nodes per tree (T3), maximum depth of the tree (T4), minimum terminal node (T5) must be selected effectively in the analyzes made with the TreeNet method. The values of these parameters directly affect the performance of the method. In the study, the optimum values of the parameters for the TreeNet method were determined by the trial-and-error method. T1, T3, T4, and T5 parameters were selected between 0.5 and 1.0, 1–10, 10000–50000, and 1–10 respectively, while the T2 parameter was selected as 10000. The performance statistics of the TreeNet method for different values of the parameters are given in Table 6. The best model found for the training dataset was then used to generate validation and test datasets, and the

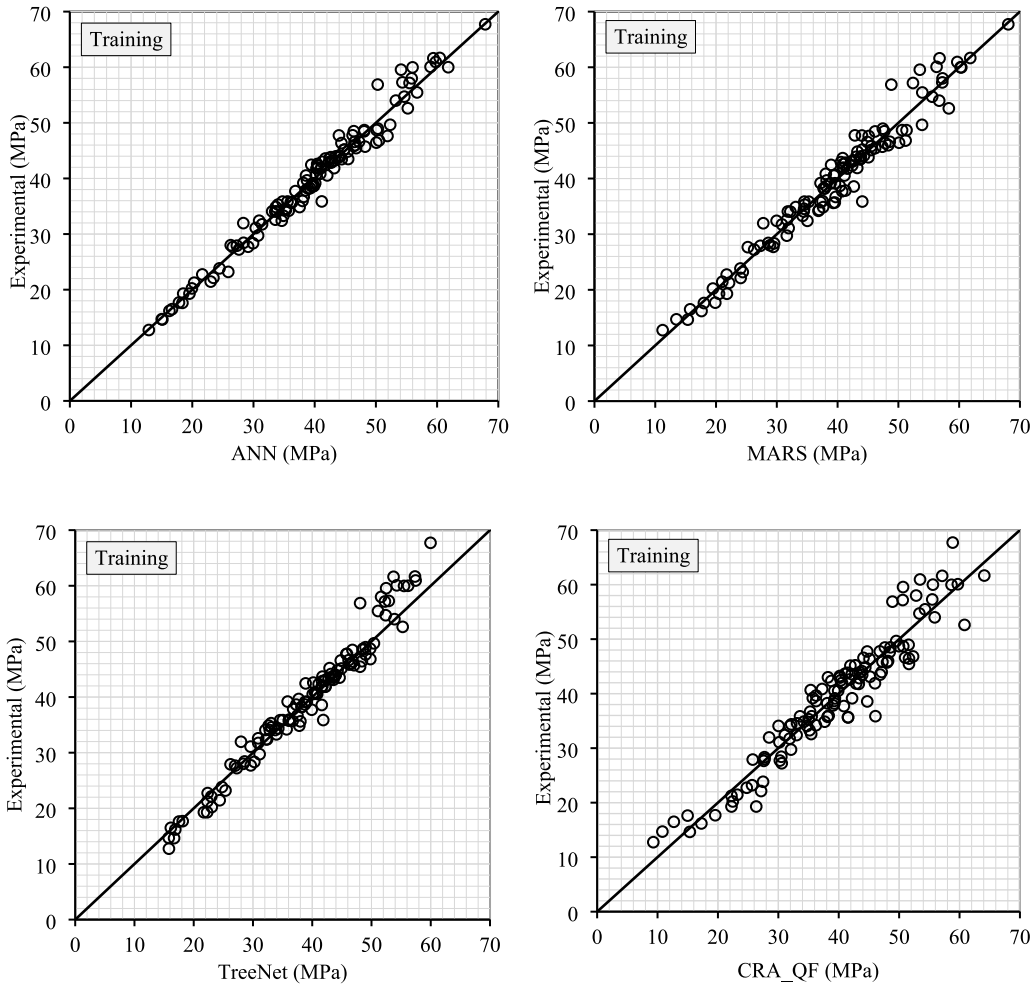

Fig. 8. Scatter plots of the experimental results with the estimated ones by the CRA-QF, TreeNet, MARS and ANN for training data sets for CS.

prediction performance of the model was compared with other models.

4.2.4. Artificial neural network (ANN) modeling results

In the ANN method, the optimum number of neurons in the hidden layer was found by the trial-and-error method. The maximum number of iterations was chosen as 10,000. The hyperbolic tangent sigmoid transfer function (tansig) and linear transfer function (purelin) are used for the activation of the hidden and output layers of the network, respectively. In the ANN models, the learning rate is 0.8 and the momentum coefficient is 1.0. The performance statistics of the ANN method for different neuron numbers in the hidden layer are given in Table 7. The best-performing ANN model is illustrated in bold.

4.2.5. Comparison of CRA, MARS and TreeNet modeling results with ANN results

In this section, the statistics of the highest-performing models of the regression-based CRA, MARS, and TreeNet methods are compared with the performance statistics obtained from the ANN method. RMSE, MAE, SI, and NS values of the models are given in Table 8 for training, validation, and testing data sets. The results with the lowest error values and the highest NS values are illustrated in bold.

The lowest RMSE and SI values for all three of the training, validation, and testing datasets were obtained from the ANN method. The lowest MAE value was obtained from the ANN method for the training and test datasets, and the MARS method for the validation dataset. It is possible to say that the ANN is the method that gives the highest performance for all data sets. The ANN method was followed by MARS, TreeNET, and CRA-QF methods, respectively. In addition, among the functions in the CRA method, it was determined that the quadratic function outperformed linear, power, and exponential functions in all training, validation, and test data sets. In the ANN method, the RMSE, MAE, SI, and NS values for the training set were determined as 1.768, 1.324, 0.045, and 0.977, respectively. When the RMSE values of the training data were examined, it was determined that the ANN model was 24.7, 28.6, and 47.5 % better than MARS, TreeNet, and CRA-QF, respectively. These values were found to be 2.1, 10.8, and 35.9 % for the validation data set, and 13.7, 19.2, and 24.9 % for the test set, respectively. When the training, validation, and test set prediction performances of the methods were compared according to their NS values, it was determined that the NS value calculated for all methods was above 0.75 and the NS values of all methods were in the “very good” class.

Scatter diagrams of ANN, MARS, TreeNet, and CRA-QF (best model of CRA) models are shown in Figs. 8-10 for training, validation, and test datasets, respectively. When the Figs. 8-10 are examined, and it is seen that the values closest to the 45° line in all the training, validation, and test data sets were obtained from the ANN, MARS, TreeNet, and CRA_QF models, respectively.

The experimental values of CS were compared with the predicted values obtained from the ANN method, where the highest performance

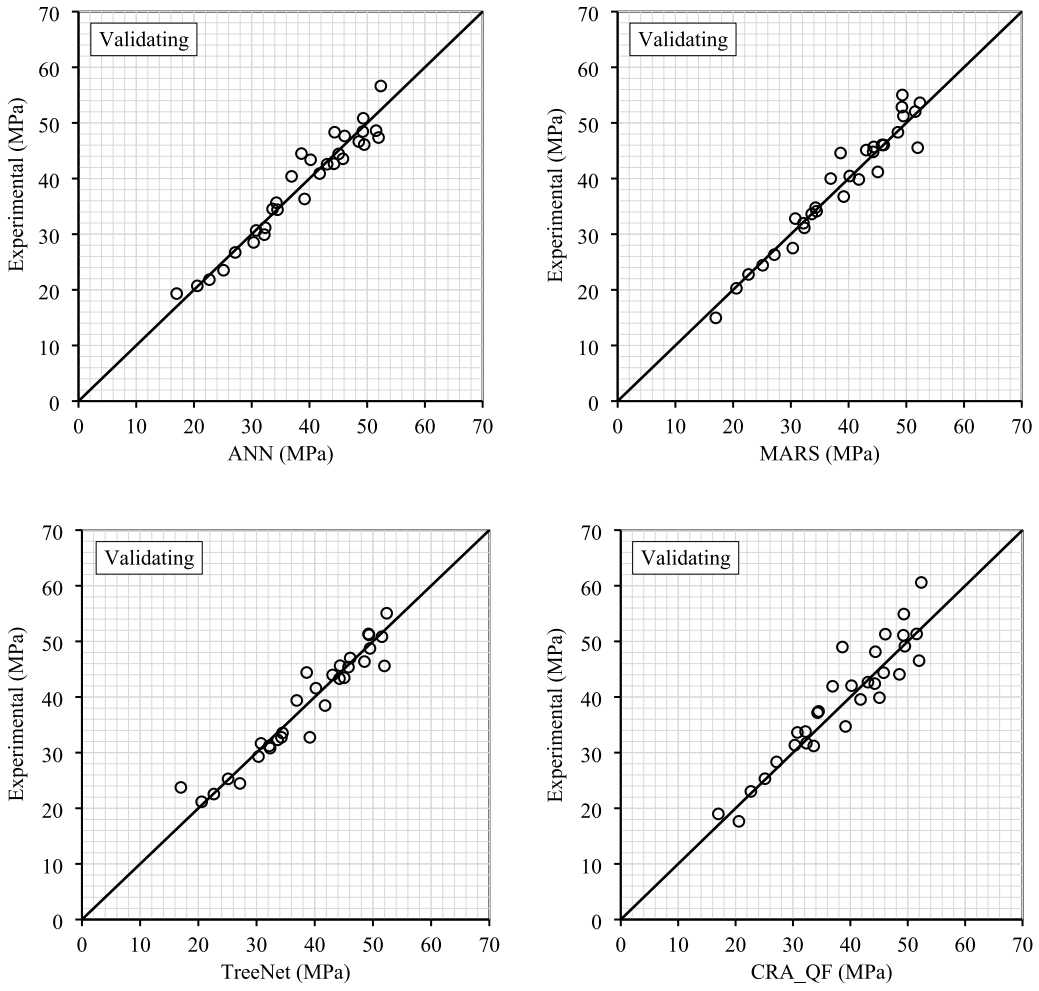

Fig. 9. Scatter plots of the experimental results with the estimated ones by the ANN, MARS, TreeNet and CRA-QF for validating data sets for CS.

values were obtained, with the time series diagrams in Figs. 11-13 for training, validation, and test data sets, respectively.

The results from the modeling study show that there is clearly a significant correlation between the experimental and predictive results for all of the training, validating, and testing data. Among the models trained using experimental data, the method that comprehensively estimated the target values was ANN. The scatter diagrams and time series given above confirm this. This shows that the models developed by ANN make more effective and better predictions compared to the regression-based models. Similar results were also obtained in [42,90] studies. The statistics given in Table 8 show that the MARS and TreeNet models predict more accurately than the CRA model. These results were similar to previous studies using similar methods [40,41]. The results given above show that ANN performs more reasonably than other methods in estimating the CS of geopolymer concrete. When the results obtained from the presented study were compared with the results obtained from the ANN models used in different studies, it was determined that the ANN once again showed superior performance in the estimation of compressive strength [37,54,91,92].

4.2.6. *Relative importance of the input variables*

MARS and TreeNet methods used in the study determine the relative importance of any independent variable by assigning a value between 0 and 100. The relative importance values obtained from the models with the highest prediction performance of the MARS and TreeNet methods are given in Table 9.

According to the results given in Table 9, it was seen that all the input variables were effective on the models established by MARS and TreeNet methods. When compared with other input parameters, the relative importance value of the curing temperature was found to be the highest. This was followed by perlite replacement ratio, molarity, and curing time, respectively. It is also supported by this modeling study that the curing temperatures significantly affect the CS of geopolymer mortars. It is also seen that the order of importance of the parameters for both MARS and TreeNet methods is the same. The relative importance of curing time was determined at the lowest level for both models. It has been determined that the relative importance of the molarity and curing time variables in the MARS method is lower than in the TreeNet method.

5. Conclusion

In this study, 540 cubic geopolymer samples incorporating different raw perlite powder (RPP) replacement ratios, different sodium hydroxide (NaOH) molarity, different curing time, and different curing temperatures for a total of 180 mixture groups were produced and their CS results were experimentally determined. Regression-based conventional regression analysis (CRA), multivariate adaptive regression splines (MARS), and TreeNet methods, as well as artificial neural network (ANN) methods, were used to predict the CS results of geopolymers using the experimental data. The key outcomes of the study

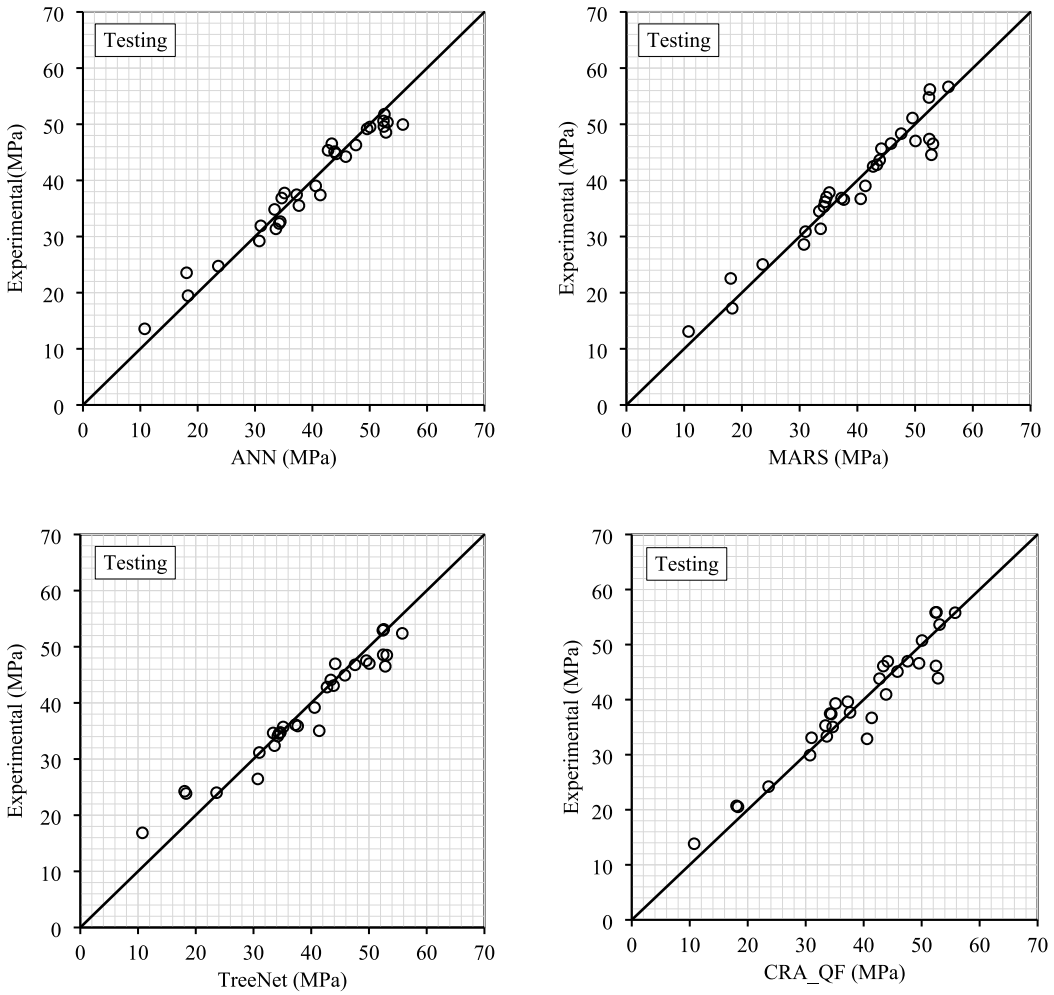

Fig. 10. Scatter plots of the experimental results with the estimated ones by the ANN, MARS, TreeNet and CRA-QF for testing data sets for CS.

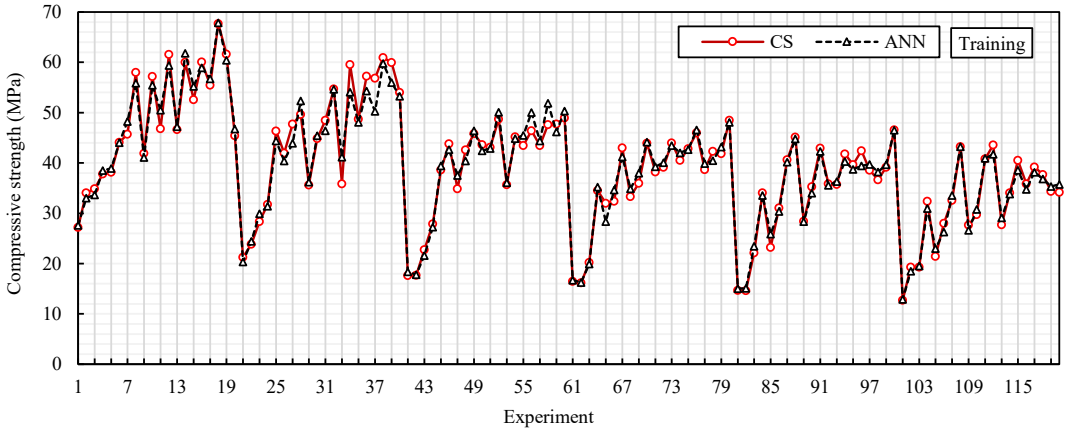

Fig. 11. Comparison of the experimental CS values with the predicted ones by the ANN for training sets.

are as follows:

- The compressive strengths of geopolymers enhance with increasing molar ratios at low-temperature curing. This is because the geopolymerization process increases with the increase in molarity. This can be attributed to more Si and Al dissolving from aluminosilicate precursors, and the chemical geopolymerization process is enhanced with high molarity. The same effect was not observed at high curing temperatures. The reason for this situation is the destruction of the geopolymer structure at high-temperature curing.
- RPP has a positive effect on CS at only low curing temperatures. The same effect was not observed at high curing temperatures. This

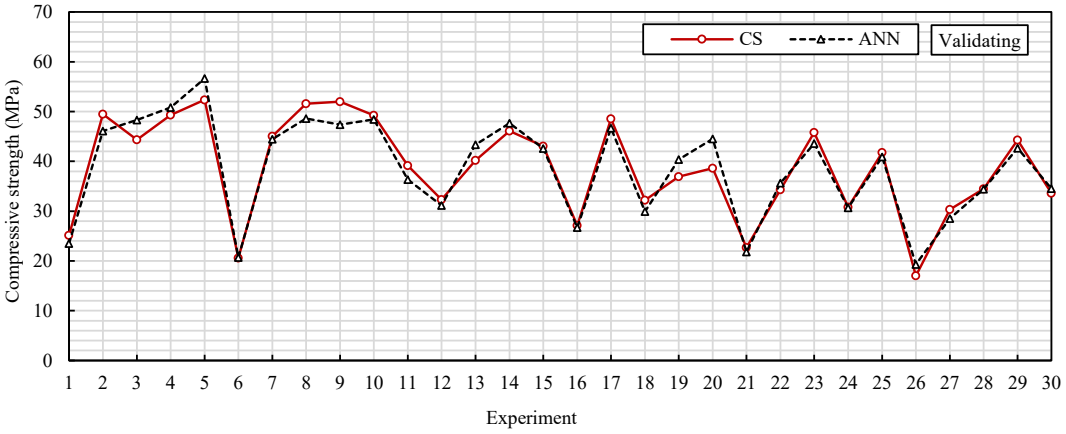

Fig. 12. Comparison of the experimental CS values with the predicted ones by the ANN for validating sets.

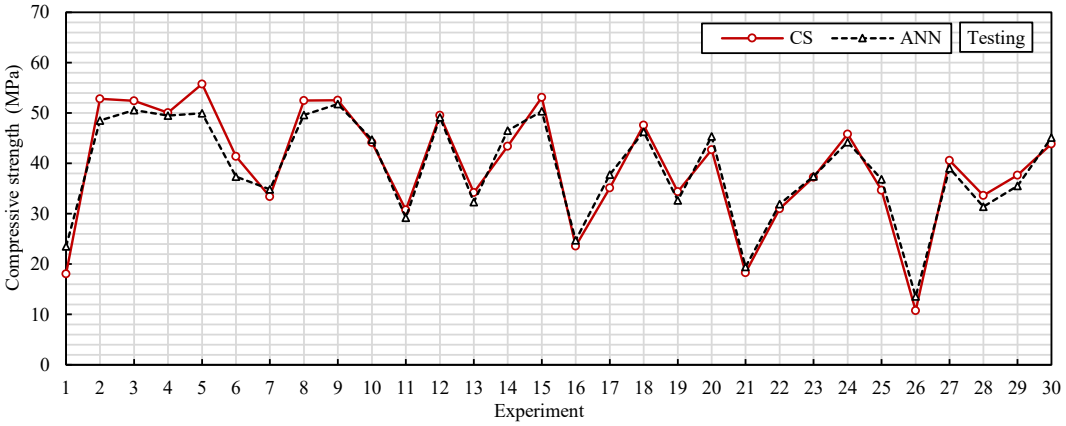

Fig. 13. Comparison of the experimental CS values with the predicted ones by the ANN for testing sets.

Table 9
Relative importance of the input variables on CS in the MARS and TreeNet.

Variable importance for MARS			Variable importance for TreeNet		
Variable name*	(%)		Variable name	(%)	
T	100		T	100	
P	84.97		P	87.7	
M	50.82		M	83.37	
H	32.82		H	63.85	

* T, H, M, and P represent curing temperatures, curing times, molarity, and perlite, respectively.

demonstrates that the degree of geopolymerization of GBFS is much higher than that of RPP.

- The NS values of the best models of all methods were found to be in the "very good" class. However, according to all performance statistics of the models, it was determined that the highest accuracy results were obtained from the ANN method. In addition, the MARS method outperformed the TreeNet and CRA methods in regression-based methods. Considering the RMSE values, it was seen that the ANN model made improvements by 24.7, 2.1, and 13.7 %, respectively, compared to the MARS method for training, validation, and test data sets.
- The variable with the highest (lowest) relative importance in the prediction of CS in the MARS and TreeNet models was the curing temperature (curing time). It was determined that these results coincided with the findings obtained from experimental studies.

This is a comprehensive study in which regression and ANN-based methods are presented comparatively for the prediction of the CS variable. It is thought that the findings obtained from this study can guide researchers. Using the same data sets, heuristic and metaheuristic algorithms can be used to investigate the feasibility of higher-performance prediction models.

CRediT authorship contribution statement

Erdinc Halis Alakara: Conceptualization, Writing – original draft. **Sinan Nacar:** Conceptualization, Writing – original draft. **Ozer Sevim:** Writing – review & editing, Validation, Methodology, Supervision. **Serdar Korkmaz:** . **Ilhami Demir:** Methodology, Supervision.

Declaration of Competing Interest

The authors declare that they have no known competing financial interests or personal relationships that could have appeared to influence

the work reported in this paper.

Data availability

Data will be made available on request.

Acknowledgment

The fourth and fifth authors gratefully acknowledge the financial assistance of the Kırıkkale University Scientific Research Centre provided under Project: 2021/112.

References

[1] J. Wei, K. Cen, Empirical assessing cement CO_2 emissions based on China's economic and social development during 2001–2030, Sci. Total Environ. 653 (2019) 200–211, https://doi.org/10.1016/j.scitotenv.2018.10.371.
[2] J.F. Xie, Y.X. Huang, W.W. Li, X.N. Song, L. Xiong, H.Q. Yu, Efficient electrochemical CO_2 reduction on a unique chrysanthemum-like Cu nanoflower electrode and direct observation of carbon deposite, Electrochim. Acta 139 (2014) 137–144, https://doi.org/10.1016/j.electacta.2014.06.034.
[3] Y.M. Amran, R. Alyousef, H. Alabduljabbar, M. El-Zeadani, Clean production and properties of geopolymer concrete; A review, J. Cleaner Prod. 251 (2020), 119679, https://doi.org/10.1016/j.jclepro.2019.119679.
[4] H. Uluyol, M.F. Gunal, I.O. Yaman, G. Yildirim, M. Sahmaran, Effects of self-healing on the microstructure, transport, and electrical properties of 100% construction- and demolition-waste-based geopolymer composites, Cem. Concr. Compos. 121 (2021), 104081, https://doi.org/10.1016/j.cemconcomp.2021.104081.
[5] J. Davidovits, Geopolymers and geopolymeric materials, J. Therm. Anal. Calorim. 35 (2) (1989) 429–441, https://doi.org/10.1007/BF01904446.
[6] J. Davidovits, Geopolymers inorganic polymeric new materials, J. Therm. Anal. Calorim. 37 (8) (1991) 1633–1656, https://doi.org/10.1007/bf01912193.
[7] M. Alhawat, A. Ashour, G. Yildirim, A. Aldemir, M. Sahmaran, Properties of geopolymers sourced from construction and demolition waste: A review, J. Build. Eng. 50 (2022), 104104, https://doi.org/10.1016/j.jobe.2022.104104.
[8] R.S. Krishna, J. Mishra, M. Zribi, F. Adeniyi, S. Saha, S. Baklouti, F.U.A. Shaikh, H. S. Gökçe, A review on developments of environmentally friendly geopolymer technology, Materialia 20 (2021), 101212, https://doi.org/10.1016/j.mtla.2021.101212.
[9] M. Lahoti, P. Narang, K.H. Tan, E.H. Yang, Mix design factors and strength prediction of metakaolin-based geopolymer, Ceram. Int. 43 (14) (2017) 1433–11144, https://doi.org/10.1016/j.ceramint.2017.06.006.
[10] O. Şahin, H. İlcan, A.T. Ateşli, A. Kul, G. Yıldırım, M. Şahmaran, construction and demolition waste-based geopolymers suited for use in 3-dimensional additive manufacturing, Cem. Concr. Compos. 121 (2021), 104088, https://doi.org/10.1016/j.cemconcomp.2021.104088.
[11] M. Rostami, K. Behfarnia, The effect of silica fume on durability of alkali activated slag concrete, Constr. Build. Mater. 134 (2017) 262–268, https://doi.org/10.1016/j.conbuildmat.2016.12.072.
[12] H. Ulugöl, A. Kul, G. Yıldırım, M. Şahmaran, A. Aldemir, D. Figueira, A. Ashour, Mechanical and microstructural characterization of geopolymers from assorted construction and demolition waste-based masonry and glass, J. Cleaner Prod. 280 (2021), 124358, https://doi.org/10.1016/j.jclepro.2020.124358.
[13] H. Ilcan, O. Sahin, A. Kul, G. Yildirim, M. Sahmaran, Rheological properties and compressive strength of construction and demolition waste-based geopolymer mortars for 3D-Printing, Constr. Build. Mater. 328 (2022), 127114, https://doi.org/10.1016/j.conbuildmat.2022.127114.
[14] H. Gökçe, M. Tuyan, M. Nehdi, Alkali-activated and geopolymer materials developed using innovative manufacturing techniques: A critical review, Constr. Build. Mater. 303 (2021), 124483, https://doi.org/10.1016/j.conbuildmat.2021.124483.
[15] S. Dadsetan, H. Siad, M. Lachemi, M. Sahmaran, Construction and demolition waste in geopolymer concrete technology: a review, Mag. Concr. Res. 71 (23) (2019) 1232–1252, https://doi.org/10.1680/jmacr.18.00307.
[16] O. Mahmoodi, H. Siad, M. Lachemi, S. Dadsetan, M. Sahmaran, Optimization of brick waste-based geopolymer binders at ambient temperature and pre-targeted chemical parameters, J. Cleaner Prod. 268 (2020), 122285, https://doi.org/10.1016/j.jclepro.2020.122285.
[17] S. Dadsetan, H. Siad, M. Lachemi, O. Mahmoodi, M. Sahmaran, Development of ambient cured geopolymer binders based on brick waste and processed glass waste, Environ. Sci. Pollut. Res. (2022), https://doi.org/10.1007/s11356-022-21469-3.
[18] P. Duxson, J.L. Provis, G.C. Lukey, J.S. Van Deventer, The role of inorganic polymer technology in the development of 'green concrete', Cem. Concr. Res. 37 (12) (2007) 1590–1597, https://doi.org/10.1016/j.cemconres.2007.08.018.
[19] O. Mahmoodi, H. Siad, M. Lachemi, S. Dadsetan, M. Sahmaran, Development of normal and very high strength geopolymer binders based on concrete waste at ambient environment, J. Cleaner Prod. 279 (2021), 123436, https://doi.org/10.1016/j.jclepro.2020.123436.
[20] A. Fernández-Jiménez, A. Palomo, Composition and microstructure of alkali activated fly ash binder: Effect of the activator, Cem. Concr. Res. 35 (10) (2005) 1984–1992, https://doi.org/10.1016/j.cemconres.2005.03.003.
[21] B. Singh, G. Ishwarya, M. Gupta, S.K. Bhattacharyya, Geopolymer concrete: A review of some recent developments, Constr. Build. Mater. 85 (2015) 78–90, https://doi.org/10.1016/j.conbuildmat.2015.03.036.
[22] J. Skibsted, M.D. Andersen, H. Jennings, The effect of alkali ions on the incorporation of aluminum in the calcium silicate hydrate (C–S–H) phase resulting from Portland cement hydration studied by ^{29}Si MAS NMR, J. Am. Ceram. Soc. 96 (2) (2013) 651–656, https://doi.org/10.1111/jace.12024.
[23] M. Olivia, H. Nikraz, Properties of fly ash geopolymer concrete designed by Taguchi method, Mater. Des. 36 (2012) 191–198, https://doi.org/10.1016/j.matdes.2011.10.036.
[24] C.E. White, J.L. Provis, T. Proffen, J.S. Van Deventer, The effects of temperature on the local structure of metakaolin-based geopolymer binder: A neutron pair distribution function investigation, J. Am. Ceram. Soc. 93 (10) (2010) 3486–3492, https://doi.org/10.1111/j.1551-2916.2010.03906.x.
[25] O. Ozturk, Engineering performance of reinforced lightweight geopolymer concrete beams produced by ambient curing, Struct. Concr. 23 (4) (2022) 2076–2082, https://doi.org/10.1002/suco.202000664.
[26] A. Noushini, A. Castel, The effect of heat-curing on transport properties of low-calcium fly ash-based geopolymer concrete, Constr. Build. Mater. 112 (2016) 464–477, https://doi.org/10.1016/j.conbuildmat.2016.02.210.
[27] P. Pavithra, M.S. Reddy, P. Dinakar, B.H. Rao, B.K. Satpathy, A.N. Mohanty, A mix design procedure for geopolymer concrete with fly ash, J. Cleaner Prod. 133 (2016) 117–125, https://doi.org/10.1016/j.jclepro.2016.05.041.
[28] H. Eskandari-Naddaf, R. Kazemi, ANN prediction of cement mortar compressive strength, influence of cement strength class, Constr. Build. Mater. 138 (2017) 1–11, https://doi.org/10.1016/j.conbuildmat.2017.01.132.
[29] A.K. Al-Shamiri, J.H. Kim, T.F. Yuan, Y.S. Yoon, Modeling the compressive strength of high-strength concrete: An extreme learning approach, Constr. Build. Mater. 208 (2019) 204–219, https://doi.org/10.1016/j.conbuildmat.2019.02.165.
[30] J. Zhang, G. Ma, Y. Huang, J. sun, F. Aslani, B. Nener, Modelling uniaxial compressive strength of lightweight self-compacting concrete using random forest regression, Constr. Build. Mater. 210 (2019) 713–719, https://doi.org/10.1016/j.conbuildmat.2019.03.189.
[31] A. Ashrafian, F. Shokri, M.J.T. Amiri, Z.M. Yaseen, M. Rezaie-Balf, Compressive strength of Foamed Cellular Lightweight Concrete simulation: New development of hybrid artificial intelligence model, Constr. Build. Mater. 230 (2020), 117048, https://doi.org/10.1016/j.conbuildmat.2019.117048.
[32] P.G. Asteris, V.G. Mokos, Concrete compressive strength using artificial neural networks, Neural. Comput. Appl. 32 (15) (2020) 11807–11826, https://doi.org/10.1007/s00521-019-04663-2.
[33] M.J. Moradi, M. Khaleghi, J. Salimi, V. Farhangi, A.M. Ramezanianpour, Predicting the compressive strength of concrete containing metakaolin with different properties using ANN, Measurement 183 (2021), 109790, https://doi.org/10.1016/j.measurement.2021.109790.
[34] F. Farooq, W. Ahmed, A. Akbar, F. Aslam, R. Alyousef, Predictive modeling for sustainable high-performance concrete from industrial wastes: A comparison and optimization of models using ensemble learners, J. Cleaner Prod. 292 (2021), 126032, https://doi.org/10.1016/j.jclepro.2021.126032.
[35] M.A. Khan, A. Zafar, F. Farooq, M.F. Javed, R. Alyousef, H. Alabduljabbar, M. I. Khan, Geopolymer concrete compressive strength via artificial neural network, adaptive neuro fuzzy interface system, and gene expression programming with K-fold cross validation, Front. Mater. 8 (2021), 621163, https://doi.org/10.3389/fmats.2021.621163.
[36] A.A. Shahmansouri, H.A. Bengar, S. Ghanbari, Compressive strength prediction of eco-efficient GGBS-based geopolymer concrete using GEP method, J. Build. Eng. 31 (2020), 101326, https://doi.org/10.1016/j.jobe.2020.101326.
[37] E.M. Golafshani, A. Behnood, M. Arashpour, Predicting the compressive strength of normal and High-Performance Concretes using ANN and ANFIS hybridized with Grey Wolf Optimizer, Constr. Build. Mater. 232 (2020), 117266, https://doi.org/10.1016/j.conbuildmat.2019.117266.
[38] S.A. Emamian, H. Eskandari-Naddaf, Genetic programming based formulation for compressive and flexural strength of cement mortar containing nano and micro silica after freeze and thaw cycles, Constr. Build. Mater. 241 (2020), 118027, https://doi.org/10.1016/j.conbuildmat.2020.118027.
[39] S. Karasu, M. Kankal, M.S. Nacar, E. Uzlu, Ö. Yüksek, Prediction of Parameters which Affect Beach Nourishment Performance Using MARS, TLBO, and Conventional Regression Techniques, Thalassas 36 (1) (2020) 245–260, https://doi.org/10.1007/s41208-019-00173-z.
[40] S. Nacar, B. Mete, A. Bayram, Estimation of daily dissolved oxygen concentration for river water quality using conventional regression analysis, multivariate adaptive regression splines, and TreeNet techniques, Environ. Monit. Assess. 192 (12) (2020) 1–21, https://doi.org/10.1007/s10661-020-08649-9.
[41] S. Tiryaki, H. Tan, S. Bardak, M. Kankal, S. Nacar, H. Peker, Performance evaluation of multiple adaptive regression splines, teaching–learning based optimization and conventional regression techniques in predicting mechanical properties of impregnated wood, Eur. J. Wood Wood Prod. 77 (4) (2019) 645–659, https://doi.org/10.1007/s00107-019-01416-9.
[42] A. Mardani-Aghabaglou, M. Kankal, S. Nacar, B. Felekoğlu, K. Ramyar, Assessment of cement characteristics affecting rheological properties of cement pastes, Neural. Comput. Appl. 33 (19) (2021) 12805–12826, https://doi.org/10.1007/s00521-021-05925-8.
[43] J.H. Fridedman, Multivariate adaptive regression splines, Ann. Statist. 19 (1) (1991) 79–141, https://doi.org/10.1214/aos/1176347963.
[44] S. Dutta, A.R. Murthy, D. Kim, P. Samui, Prediction of compressive strength of self-compacting concrete using intelligent computational modeling, Comput. Mater. Contin. 53 (2) (2017) 167–185.

[45] W. Zhang, A.T.C. Goh, Multivariate adaptive regression splines and neural network models for prediction of pile drivability, Geosci. Front. 7 (1) (2016) 45–52, https://doi.org/10.1016/j.gsf.2014.10.003.
[46] Y. Lin, C.P. Lai, T. Yen, Prediction of ultrasonic pulse velocity (UPV) in concrete, ACI Mater. J. 100 (1) (2003) 21–28.
[47] G.F. Kheder, A two stage procedure for assessment of in situ concrete strength using combined non-destructive testing, Mater. Struct. 32 (6) (1999) 410–417, https://doi.org/10.1007/BF02482712.
[48] G. Trtnik, F. Kavčič, G. Turk, Prediction of concrete strength using ultrasonic pulse velocity and artificial neural networks, Ultrasonics 49 (1) (2009) 53–60, https://doi.org/10.1016/j.ultras.2008.05.001.
[49] T. Gupta, M.C. Rao, Prediction of compressive strength of geopolymer concrete using machine learning techniques, Struct. Concr. (2021), https://doi.org/10.1002/suco.202100354.
[50] G.F. Huseien, I. Faridmehr, M.L. Nehdi, A.A. Abadel, T.A. Aiken, S.K. Ghoshal, Structure, morphology and compressive strength of Alkali-activated mortars containing waste bottle glass nanoparticles, Constr. Build. Mater. 342 (2022), 128005, https://doi.org/10.1016/j.conbuildmat.2022.128005.
[51] H.G. Ni, J.Z. Wang, Prediction of compressive strength of concrete by neural networks, Cem. Concr. Res. 30 (8) (2000) 1245–1250, https://doi.org/10.1016/S0008-8846(00)00345-8.
[52] K.T. Nguyen, Q.D. Nguyen, T.A. Le, J. Shin, K. Lee, Analyzing the compressive strength of green fly ash based geopolymer concrete using experiment and machine learning approaches, Constr. Build. Mater. 247 (2020), 118581, https://doi.org/10.1016/j.conbuildmat.2020.118581.
[53] M. Rahmati, V. Toufigh, Evaluation of geopolymer concrete at high temperatures: An experimental study using machine learning, J. Cleaner Prod. 372 (2022), 133608, https://doi.org/10.1016/j.jclepro.2022.133608.
[54] A.C. Ganesh, M. Muthukannan, Development of high performance sustainable optimized fiber reinforced geopolymer concrete and prediction of compressive strength, J. Cleaner Prod. 282 (2021), 124543, https://doi.org/10.1016/j.jclepro.2020.124543.
[55] P. Manikandan, V. Vasugi, Potential utilization of waste glass powder as a precursor material in synthesizing ecofriendly ternary blended geopolymer matrix, J. Cleaner Prod. 355 (2022), 131860, https://doi.org/10.1016/j.jclepro.2022.131860.
[56] M. Ahmad, K. Rashid, Z. Tariq, M. Ju, Utilization of a novel artificial intelligence technique (ANFIS) to predict the compressive strength of fly ash-based geopolymer, Constr. Build. Mater. 301 (2021), 124251, https://doi.org/10.1016/j.conbuildmat.2021.124251.
[57] J. Britto, M.P. Muthuraj, Prediction of compressive strength of bacteria incorporated geopolymer concrete by using ANN and MARS, Struct. Eng. Mech. 70 (6) (2019) 671–681, https://doi.org/10.12989/sem.2019.70.6.671.
[58] T.T. Pham, T.T. Nguyen, L.N. Nguyen, P.V. Nguyen, A neural network approach for predicting hardened property of geopolymer concrete, Int. J. GEOMATE 19 (74) (2020) 176–184, https://doi.org/10.21660/2020.74.
[59] P. Duxson, J.L. Provis, G.C. Lukey, S.W. Mallicoat, W.M. Kriven, J.S.J. van Deventer, Understanding the relationship between geopolymer composition, microstructure and mechanical properties, Colloids Surf., A 269 (1–3) (2005) 47–58, https://doi.org/10.1016/j.colsurfa.2005.06.060.
[60] R.A. Robayo-Salazar, W. Valencia-Saavedra, R. Mejía de Gutiérrez, Construction and demolition waste (CDW) recycling—as both binder and aggregates—in alkali-activated materials: a novel Re-use concept, Sustainability 12 (14) (2020) 5775, https://doi.org/10.3390/su12145775.
[61] K. Parthiban, K. Saravanarajamohan, S. Shobana, A.A. Bhaskar, Effect of replacement of slag on the mechanical properties of fly ash based geopolymer concrete, Int. J. Eng. Technol. 5 (3) (2013) 2555–2559.
[62] E. Kamseu, L.B. Moungam, M. Cannio, N. Billong, D. Chaysuwan, U.C. Meloand, C. Leoelli, Substitution of sodium silicate with rice husk ash-NaOH solution in metakaolin based geopolymer cement concerning reduction in global warming, J. Cleaner Prod. 142 (2017) 3050–3060, https://doi.org/10.1016/j.jclepro.2016.10.164.
[63] TS EN 196-1, Methods of testing cement–Part 1: Determination of strength, Turkish Standard Institution, Ankara, (2016).
[64] P. Duxson, J.L. Provis, Designing precursors for geopolymer cements, J. Am. Ceram. Soc. 91 (12) (2008) 3864–3869, https://doi.org/10.1111/j.1551-2916.2008.02787.x.
[65] Astm C109, C109M-21, Standard Test Method for Compressive Strength of Hydraulic Cement Mortars (Using 2-in. or [50-mm] Cube Specimens), ASTM International, West Conshohocken, PA, 2021.
[66] N.A. Jaya, L. Yun-Ming, H. Cheng-Yong, M.M.A.B. Abdullah, K. Hussin, Correlation between pore structure, compressive strength and thermal conductivity of porous metakaolin geopolymer, Constr. Build. Mater. 247 (2020), 118641, https://doi.org/10.1016/j.conbuildmat.2020.118641.
[67] P. Rovnaník, Effect of curing temperature on the development of hard structure of metakaolin-based geopolymer, Constr. Build. Mater. 24 (7) (2010) 1176–1183, https://doi.org/10.1016/j.conbuildmat.2009.12.023.
[68] G. Görhan, G. Kürklü, The influence of the NaOH solution on the properties of the fly ash-based geopolymer mortar cured at different temperatures, Composites, Part B 58 (2014) 371–377, https://doi.org/10.1016/j.compositesb.2013.10.082.
[69] N.V. K, D.L.V. Babu, Assessing the performance of molarity and alkaline activator ratio on engineering properties of self-compacting alkaline activated concrete at ambient temperature, J. Build. Eng. 20 (2018) 137–155, https://doi.org/10.1016/j.jobe.2018.07.005.
[70] M.H. Al-Majidi, A. Lampropoulos, A. Cundy, S. Meikle, Development of geopolymer mortar under ambient temperature for in situ applications, Constr. Build. Mater. 120 (2016) 198–211, https://doi.org/10.1016/j.conbuildmat.2016.05.085.
[71] A. Hassan, M. Arif, M. Shariq, Use of geopolymer concrete for a cleaner and sustainable environment–A review of mechanical properties and microstructure, J. Cleaner Prod. 223 (2019) 704–728, https://doi.org/10.1016/j.jclepro.2019.03.051.
[72] L. Biondi, M. Perry, C. Vlachakis, Z. Wu, A. Hamilton, J. McAlorum, Ambient cured fly ash geopolymer coatings for concrete, Materials 12 (6) (2019) 923, https://doi.org/10.3390/ma12060923.
[73] W. Huo, Z. Zhu, W. Chen, J. Zhang, Z. Kang, S. Pu, Y. Wan, Effect of synthesis parameters on the development of unconfined compressive strength of recycled waste concrete powder-based geopolymers, Constr. Build. Mater. 292 (2021), 123264, https://doi.org/10.1016/j.conbuildmat.2021.123264.
[74] D. Panias, I.P. Giannopoulou, T. Perraki, Effect of synthesis parameters on the mechanical properties of fly ash-based geopolymers, Colloids Surf., A 301 (1–3) (2007) 246–254, https://doi.org/10.1016/j.colsurfa.2006.12.064.
[75] A. Bayram, E. Uzlu, M. Kankal, T. Dede, Modeling stream dissolved oxygen concentration using teaching–learning based optimization algorithm, Environ. Earth Sci. 73 (10) (2015) 6565–6576, https://doi.org/10.1007/s12665-014-3876-3.
[76] T.M.D.K. Bandara, R.D. Yapa, S.R. Kodituwakku, Simulation of regression analysis by an automated system utilizing artificial neural networks, Int. J. Latest Trends Comput. 2 (3) (2011) 378.
[77] B. Yilmaz, E. Aras, S. Nacar, M. Kankal, Estimating suspended sediment load with multivariate adaptive regression spline, teaching-learning based optimization, and artificial bee colony models, Sci. Total Environ. 639 (2018) 826–840, https://doi.org/10.1016/j.scitotenv.2018.05.153.
[78] O. Kisi, K.S. Parmar, Application of least square support vector machine and multivariate adaptive regression spline models in long-term prediction of river water pollution, J. Hydrol. 534 (2016) 104–112, https://doi.org/10.1016/j.jhydrol.2015.12.014.
[79] M. Zabihi, H.R. Pourghasemi, Z.S. Pourtaghi, M. Behzadfar, GIS-based multivariate adaptive regression spline and random forest models for groundwater potential mapping in Iran, Environ. Earth Sci. 75 (2016) 665, https://doi.org/10.1007/s12665-016-5424-9.
[80] J.H. Friedman, Greedy function approximation: a gradient boosting machine, Ann. Stat. 29 (2001) 1189–1232.
[81] L. Chen, S. Peng, B. Yang, Predicting alien herb invasion with machine learning models: biogeographical and life-history traits both matter, Biol. Invasions 17 (7) (2015) 2187–2198, https://doi.org/10.1007/s10530-015-0870-y.
[82] Salford Predictive Modeler, Introducing TreeNet Gradient Boosting Machine, Salford Predictive Modeler by Minitab, USA, 2019.
[83] D. Hanbay, İ. Turkoglu, Y. Demir, An expert system based on wavelet decomposition and neural network for modeling Chua's circuit, Expert Sys. Appl. 34 (4) (2008) 2278–2283, https://doi.org/10.1016/j.eswa.2007.03.002.
[84] B.V. Kok, M. Yilmaz, B. Sengoz, A. Sengur, E. Avci, Investigation of complex modulus of base and SBS modified bitumen with artificial neural networks, Expert Sys. Appl. 37 (12) (2010) 7775–7780, https://doi.org/10.1016/j.eswa.2010.04.063.
[85] D.N. Moriasi, J.G. Arnold, M.W. Van Liew, R.L. Bingner, R.D. Harmel, T.L. Veith, Model evaluation guidelines for systematic quantification of accuracy in watershed simulations, Trans. ASABE 50 (2007) 885–900, https://doi.org/10.13031/2013.23153.
[86] S.T. Erdogan, Properties of ground perlite geopolymer mortars, J. Mater. Civ. Eng. 27 (7) (2015) 04014210, https://doi.org/10.1061/(ASCE)MT.1943-5533.0001172.
[87] A.S. de Vargas, D.C. Dal Molin, Â.B. Masuero, A.C. Vilela, J. Castro-Gomes, R.M. de Gutierrez, Strength development of alkali-activated fly ash produced with combined NaOH and $Ca(OH)_2$ activators, Cem. Concr. Compos. 53 (2014) 341–349, https://doi.org/10.1016/j.cemconcomp.2014.06.012.
[88] X. Guo, H. Shi, W.A. Dick, Compressive strength and microstructural characteristics of class C fly ash geopolymer, Cem. Concr. Compos. 32 (2) (2010) 142–147, https://doi.org/10.1016/j.cemconcomp.2009.11.003.
[89] P. Sukmak, S. Horpibulsuk, S.L. Shen, Strength development in clay–fly ash geopolymer, Constr. Build. Mater. 40 (2013) 566–574, https://doi.org/10.1016/j.conbuildmat.2012.11.015.
[90] U.K. Sevim, H.H. Bilgic, O.F. Cansiz, M. Ozturk, C.D. Atis, Compressive strength prediction models for cementitious composites with fly ash using machine learning techniques, Constr. Build. Mater. 271 (2021), 121584, https://doi.org/10.1016/j.conbuildmat.2020.121584.
[91] A.A. Shahmansouri, M. Yazdani, S. Ghanbari, H.A. Bengar, A. Jafari, H.F. Ghatte, Artificial neural network model to predict the compressive strength of eco-friendly geopolymer concrete incorporating silica fume and natural zeolite, J. Cleaner Prod. 279 (2021), 123697, https://doi.org/10.1016/j.jclepro.2020.123697.
[92] F. Özcan, C.D. Atiş, O. Karahan, E. Uncuoğlu, H. Tanyildizi, Comparison of artificial neural network and fuzzy logic models for prediction of long-term compressive strength of silica fume concrete, Adv. Eng. Software 40 (9) (2009) 856–863, https://doi.org/10.1016/j.advengsoft.2009.01.005.